Available online at www.sciencedirect.com
ScienceDirect
C. R. Physique 9 (2008) 130–141
COMPTES RENDUS PHYSIQUE
http://france.elsevier.com/direct/COMREN/

Recent developments in terahertz optoelectronics/Développements récents en optoélectronique térahertz

THz emission from semiconductor surfaces

Vitalij L. Malevich [a], Ramūnas Adomavičius [b], Arūnas Krotkus [b,c,*]

[a] *Institute of Physics, National Academy of Sciences of Belarus, F. Skaryna Ave. 68, 220072 Minsk, Belarus*
[b] *Semiconductor Physics Institute, 01108 Vilnius, Lithuania*
[c] *Department of Semiconductor Physics, Vilnius University, 10222 Vilnius, Lithuania*

Available online 4 January 2008

Abstract

We provide a review of experimental and theoretical work on electromagnetic terahertz pulse emission from semiconductor surfaces excited by femtosecond laser radiation. The main terahertz emission mechanisms are analysed. The terahertz emission from InAs and Ge is explained by the photo-Dember effect and electric field induced optical rectification. Electronic band structure and carrier scattering mechanisms are investigated by means of terahertz emission and absorption spectroscopy in InAs, InSb and Ge. ***To cite this article: V.L. Malevich et al., C. R. Physique 9 (2008).***

Résumé

Émission THz des surfaces de matériaux semi-conducteurs. Nous présentons une revue des travaux expérimentaux et théoriques consacrés à l'émission de rayonnement térahertz par des surfaces de matériaux semi-conducteurs éclairées par des impulsions lasers de durée femtoseconde. Les principaux mécanismes d'émission THz sont analysés. L'émission THz rayonnée par InAs et Ge est due à l'effet Dember optique associé à du redressement optique. Nous étudions la structure de bande électronique et les phénomènes de relaxation des porteurs libres dans InAs, InSb et Ge, en analysant cette émission THz de surface ainsi que des résultats de spectroscopie THz d'absorption. ***Pour citer cet article : V.L. Malevich et al., C. R. Physique 9 (2008).***

Keywords: Terahertz emission; Photo-Dember effect; Electric field induced optical rectification

Mots-clés : Émission térahertz ; Effet Dember optique ; Redressement optique

1. Introduction

There are two basic approaches for generating terahertz (THz) radiation beams from semiconductors excited by ultrashort laser pulses: the photoconductive technique, based on high speed photodetectors integrated with wide-band radiating antennae [1], and bare semiconductor surfaces illuminated by femtosecond laser beams [2]. In the case of photoconductive antennae that are used both for THz pulse generation and their detection, the main problem remaining is the availability of the proper semiconductor material that should be photosensitive at the laser wavelength and should have other distinctive properties such as high resistivity and subpicosecond carrier lifetimes. For the most popular in

* Corresponding author.
E-mail address: krotkus@pfi.lt (A. Krotkus).

1631-0705/$ – see front matter
doi:10.1016/j.crhy.2007.09.014

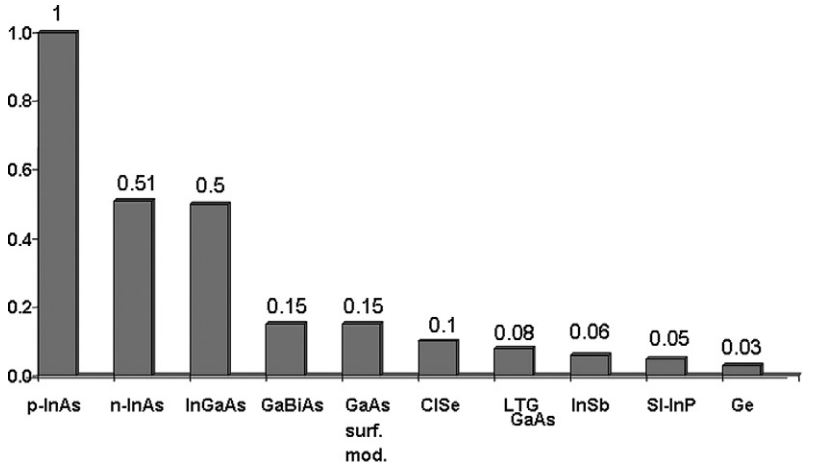

Fig. 1. THz emission from different semiconductors excited by the Ti:sapphire laser ($\lambda = 800$ nm, $\tau_{\text{imp}} = 150$ fs, $f = 76$ MHz, $I = 100$ mJ/cm^2).

THz pulse applications femtosecond laser system—mode-locked Ti:sapphire laser (laser wavelength of ∼800 nm), the material of choice is low-temperature molecular-beam-epitaxy grown GaAs (LTG GaAs) layers [3]; however, the search for the most suitable semiconductor that could be used in THz antennae activated by femtosecond lasers generating at longer wavelengths from 1 to 1.5 μm is still not finished. InGaAs [4], GaSbAs [5], and LTG GaBiAs [6] are among possible candidates for ultrafast photodetectors in this spectral range.

In the second case, when THz pulses are generated by illuminating semiconductor surfaces with ultrashort laser pulses, all restrictions mentioned above on the material properties are less important. Stronger or weaker THz pulses are emitted from the majority of weakly or moderately doped semiconductors with rather long carrier lifetimes. Fig. 1 presents a comparison of THz pulse amplitudes emitted by a number of various materials illuminated by femtosecond Ti:sapphire laser pulses. It can be seen that the best THz emitters are narrow-gap semiconductors like InAs, which have optical absorption edge corresponding to the mid-infrared spectral region. Besides the rather universal occurrence of this effect, emission from the semiconductor surfaces provides much wider and better shaped THz beams than those generated by photoconductive antennae, which could be preferable for some specific applications like THz imaging.

In the present article we will discuss physical mechanisms leading to the THz emission from the semiconductor surfaces and will compare the characteristics of this effect in various materials.

2. Terahertz emission mechanisms

Generally speaking, THz radiation at the photoexcited semiconductor surface can be emitted by a dipole that is induced either due to a fast changing photocurrent or by the nonlinear polarization of the material. In the far field region the THz field can be expressed as

$$E_{\text{THz}} = -\frac{S}{c^2 R}\int_0^\infty \left(\frac{\partial j}{\partial t} + \frac{\partial^2 P}{\partial t^2}\right) \mathrm{d}z \tag{1}$$

where c is the speed of light in vacuum, R is the distance from the point of observation to the emitting region, S is the area of the laser excited spot on the semiconductor surface; j and P are the photocurrent and nonlinear polarization components in the direction of the THz wave polarization, respectively. Integration of the relation (1) is carried out over the depth z. It is important to point out that the expression (1) is correct when the diameter of the illuminated spot is smaller then the wavelength of the emitted THz radiation, otherwise the dipole approach becomes not applicable and the THz field amplitude should be determined by summing up partial waves emitted by separate surface elements and by taking into account their phase relations. In the following we will discuss different physical mechanisms leading to the appearance of the transient photocurrent or low-frequency nonlinear polarization components entering relation (1).

2.1. Photocurrent surge

Electrons and holes that are optically generated in the semiconductor due to the interband absorption of femtosecond laser radiation are spatially separated by the built-in or external electric field, which results in a transient photocurrent varying on a subpicosecond time scale. This fast varying photocurrent can be an effective source of THz radiation with the amplitude defined by the time derivative of the photocurrent. This mechanism of THz generation is known as the photocurrent surge effect and it is realized in widely used LTG-GaAs photoconductive antennae and in THz emitters made from the semiconductors with a strong band bending at their surface. The latter case is, e.g., typical for GaAs. The surface depletion field has opposite polarities for n- and p-doped semiconductor samples; therefore, the polarities of THz pulses emitted from those samples will also be of an opposite sign.

Photocurrent transport in depletion layer is accompanied by charge redistribution and electric field screening, thus these processes should be considered self-consistently. The dynamics of photocarriers and electric field are occasionally analyzed on the basis of the self-consistent solution of drift-diffusion transport equations for electrons and holes and the Poisson equation [7]. However, the validity of this approach is questionable, because the time scale of the processes leading to THz radiation is of the order of 10^{-13} s, which is comparable with the carrier momentum and energy relaxation times in semiconductors. Thus, the drift-diffusion approximation cannot take definitely into account such effects as the electron velocity overshoot or the reactive current resulting in collision-less regime of the electric field screening.

A comprehensive description of photocarrier transport and field dynamics on a subpicosecond time scale should be performed on the basis of ensemble Monte Carlo simulations of macroparticle transport in the time-varying inhomogeneous depletion field that is found self-consistently from the Poisson equation [8]. This method allows taking into account the many-valley structure of the conduction band and a variety of carrier scattering mechanisms.

THz electric fields calculated by the Monte Carlo method for two differently doped n-GaAs samples excited by 100 fs laser pulses (photon energy is equal to 1.55 eV) are presented in Fig. 2 [9]. The shape of THz-pulse changes from bipolar to oscillatory with increasing doping level, which can be explained as a change of depletion field screening mode. For low doped semiconductor, when the condition $\omega_p\tau < 1$ (ω_p is the plasma frequency, and τ is the momentum relaxation time for electrons) is satisfied, the drift-diffusion regime is realized and the depletion electric field decreases monotonically in time (dielectric relaxation); THz waveform is bipolar in this case. At a higher doping level ($\omega_p\tau > 1$) the field screening follows the collision-less regime and the depletion field decreases oscillating with a plasma frequency. The oscillatory waveform of the THz pulses was observed experimentally by Kersting et al. [10] in highly doped n-GaAs and the effect was explained as plasma oscillations of equilibrium electrons launched by the photoexcitation. It has turned out, that the frequency of plasma oscillations does not depend on the photoexcitation

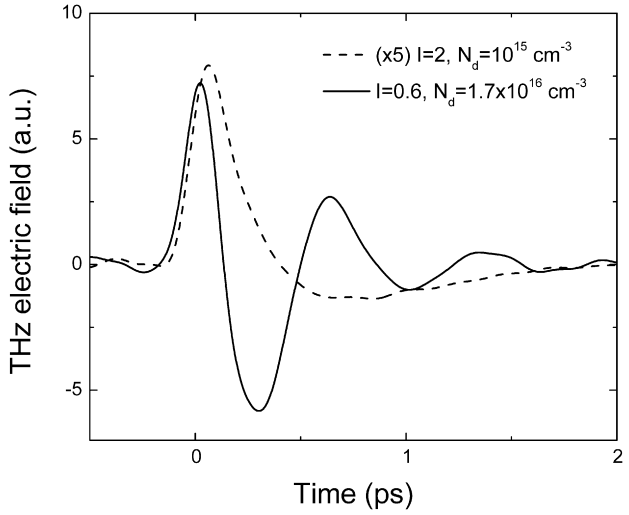

Fig. 2. Calculated waveforms of THz pulse emitted from two n-GaAs samples excited by a 100 fs laser pulse with the photon energy of 1.55 eV. The photoelectron densities at the surface were 2×10^{15} cm^{-3} and 2×10^{16} cm^{-3} for low- and high-doped samples, respectively.

level as if the photocarriers are not participating in the plasma oscillation and screening processes. This could be understood if one remembers that the 'hot' photoelectrons have higher scattering rate and effective masses than the 'cold', intrinsic electrons, and are thus less prone to participate in the plasma oscillation.

It should be pointed out that the plasma oscillations are often considered as a separate mechanism of THz emission from photoexcited semiconductor surface. In fact, this mechanism has the same origin as the photocurrent surge effect. Both these mechanisms should be considered together in terms of self-consistent dynamics of photocarrier motion and depletion field screening and the only difference between them consists in different screening regimes of the built-in depletion field.

2.2. *Photo-Dember effect*

In so-called photo-Dember effect, spatial separation of electrons and holes occurs due to their different mobilities. Photoexcited electrons diffusing from their excitation point at the surface towards the bulk of the material surpass less mobile holes and, as a result, the space charge and the electric field appear. This electric field starts to slow down the photoelectrons and to accelerate the holes; therefore, both types of photocarriers are later on moving as a single quasineutral packet. The photo-Dember effect has been, until recently, studied for the case of a stationary photoexcitation when the drift-diffusion approach is correct. In this case, the Dember photovoltage is typically low, being of the order of 10^{-2} V.

The situation changes radically when the electrons are excited by ultrashort laser pulses high in the conduction band, as it happens during irradiation of InAs or InSb by Ti:sapphire laser pulses. In this case the photoelectrons remain hot for several picoseconds after the excitation and due to their high kinetic energy ($\sim$1 eV for InAs) are propagating over distances much larger than thermal electron and hole separation lengths. Fig. 3 presents temporal dependences of the photovoltage calculated by Monte Carlo procedure for the case of n-InAs excited by 100-fs duration laser pulses with different photon energy from the range of 1.0–1.9 eV [11]. As it can be seen from this figure, surface photovoltages as large as 1 V can be achieved at the illuminated surface; it is the largest for the photon energy of $\sim$1.5 eV and steeply decreases for even larger laser energy quanta. The later observation can be explained by the onset of the photoelectron transfer to the subsidiary conduction band valleys.

It can be shown that THz electric field in the pulse can be directly expressed in terms of the surface photovoltage. Indeed, by taking into account the current continuity equation

$$\frac{\varepsilon}{4\pi}\frac{\partial F}{\mathrm{d}t} + j = 0 \tag{2}$$

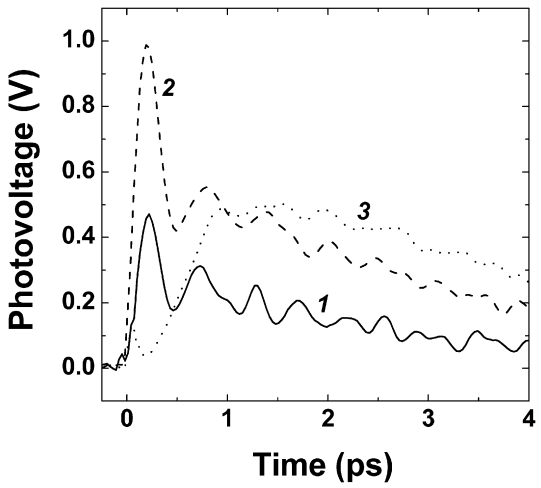

Fig. 3. Time dependencies of the surface photovoltage induced in n-InAs ($N_d = 1.8 \times 10^{16}$ cm^{-3}) by 100 fs duration laser pulses with the photon energies (1) 1.0, (2) 1.55, and (3) 1.9 eV. Curves are obtained by Monte Carlo simulations with the same excitation photon density 4×10^{12} cm^{-2}.

one can obtain from (1)

$$E_{\mathrm{THz}} = \frac{\varepsilon S}{4\pi Rc^2}\frac{\mathrm{d}^2\varphi_{\mathrm{s}}}{\mathrm{d}t^2} \tag{3}$$

Here ε is the static dielectric permittivity, F is the electric field induced by the spatial separation of photocarriers, and $\varphi_{\mathrm{s}} = \int_0^\infty F\,\mathrm{d}z$ is the surface photovoltage.

Assuming the existence of two groups of electrons (equilibrium and photoexcited) with different energies and, accordingly, different effective masses and momentum relaxation times, one can obtain for THz electric field

$$E_{\mathrm{THz}} = \frac{e\alpha W S v_0^2}{3\hbar\omega Rc^2}\mathrm{e}^{-t/\tau}\cos\omega_{\mathrm{p}}t \tag{4}$$

where α is the optical absorption coefficient, W and ω are the fluence and the frequency of exciting radiation, v_0 is the velocity of photoelectrons with kinetic energy $\varepsilon_0 \approx \hbar\omega - \varepsilon_{\mathrm{g}}$ (ε_{g} is the semiconductor forbidden gap). The relation (4) is valid in a quasi-ballistic regime ($\omega_{\mathrm{p}}\tau > 1$), and it can be used as an estimation for THz field emitted from InAs under femtosecond laser excitation with photon energy below the threshold for electron inter-valley transitions. It should be noted that the dependence of THz field on the laser energy fluence is linear only at low excitation levels. When excitation becomes higher, the photo-Dember contribution into THz field increases logarithmically with the fluence.

The photoeffect considered above was analyzed under the assumption that optically generated electrons and holes are isotropically distributed in momentum space. However, because of the specific symmetry of the hole wave functions in zinc-blende semiconductors like GaAs and InAs, the interband optical transition matrix elements have a such structure that photocarriers are distributed over momenta anisotropically. This optical alignment of photoelectron momenta was found to cause such effects as the polarization of hot luminescence [12] and the surface ballistic photoeffect [13]. The second of those effects manifests itself in the appearance of the lateral photocurrent at semiconductor surface illuminated by linearly polarized light and was investigated theoretically and experimentally in GaAs at cryogenic temperatures [14].

The lateral component of the photocurrent arising at semiconductor surface under femtosecond laser irradiation is usually lower than the perpendicular component, but due to its orientation the contribution of lateral current in THz emission can be quite considerable.

2.3. Optical rectification

In a non-centrosymmetric semiconductor the low-frequency nonlinear polarization P responsible for the optical rectification effect is given by the relation

$$P = \chi^{(2)}EE^* + \chi^{(3)}EE^*F \tag{5}$$

where E is the electric field of the exciting laser pulse, $\chi^{(2)}$ and $\chi^{(3)}$ are the second- and the third-order nonlinear optical susceptibility tensors, respectively. The first term in (5) describes the intrinsic bulk contribution into the optical rectification (OR) effect, while the second term containing the dc electric field F is responsible for the so-called electric field induced optical rectification (EFIOR) effect. The field F can be of a built-in origin, but it could also be induced due to the spatial separation of photocarriers. The main characteristic property of the optical rectification mechanism of THz generation distinguishing it from the current surge mechanisms is its azimuthal anisotropy; the type of the azimuthal angle φ dependence being different for each surface of the crystal [15]. Azimuthal angle dependences can be, therefore, used for separating the bulk OR and EFIOR contributions, because for (100) crystalline plane of a cubic crystal the first of these contributions changes proportionally to $\cos 2\varphi$, whereas the second is independent on φ [15].

By substituting (5) into (1) and by taking into account the relation $EE^* \approx 4\pi W\exp(-\alpha z)/(cn\tau_i)$ (τ_i is the laser pulse duration, n is the refractive index at the wavelength of the exciting radiation), one can obtain for THz field caused by the nonlinear optical rectification as

$$E_{\mathrm{THz}} \approx \frac{4\pi WS}{Rc^3 n\alpha\tau_i^3}\left(\chi^{(2)} + \alpha\chi^{(3)}\int_0^\infty F\mathrm{e}^{-\alpha z}\,\mathrm{d}z\right) \tag{6}$$

As follows from this expression, shortening of the excitation pulse leads to a quite sharp increase (proportional to $\sim\tau_i^{-3}$) of OR and EFIOR contributions in THz emission.

The contributions of OR and EFIOR effects in THz emission are defined by the values of nonlinear optical susceptibilities of the material. In a spectral region where the material is transparent, the nonlinear susceptibilities are mainly defined by the bond electrons; for zinc-blende semiconductors their values are of the order of $\chi^{(2)} \sim 10^{-6}$ esu, $\chi^{(3)} \sim 10^{-10}$ esu, correspondingly [16,17]. However, when the photon energies start to exceed the absorption edge the nonlinear susceptibilities can become significantly (at least by two orders of magnitude) enhanced due to the contribution of free carriers [18,19]. A comparison of photo-Dember (4) and optical rectification (6) mechanisms for InAs shows that the contribution of the first effect prevails at the excitation level lower 1 $\mu J/cm^2$. However, at higher fluence the photo-Dember effect grows logarithmically and as a result the nonlinear optical effects can exceed the photo-Dember contribution.

3. Results obtained on various semiconductors

3.1. InAs

The majority of authors have concluded that the buildup of the photo-Dember field is responsible for the emission of THz radiation in InAs, however some observations can be best explained by the influence of instantaneous polarization due to electric-field-induced optical rectification at the semiconductor surface.

Fig. 4 shows azimuthal angle dependences of the THz field amplitude measured on two n-InAs and two p-InAs (111) samples. Clear $\sin 3\varphi$ type dependence on the azimuthal angle φ were observed, and the amplitude of S-polarized THz signals measured on differently doped samples was correlating with the doping level dependence of P-polarized THz radiation presented in [20]. Photocurrent surge effects cannot lead to the generation of S-polarized signal, therefore, the observed radiation is originating either from the bulk OR effect, or from the EFIOR effect, both of which show $\sin 3\varphi$ dependence for (111) crystallographic plane [15]. Both nonlinear optical contributions can be separated by measuring azimuthal angle dependences on (100) planes; in this case the generated THz signal should be independent on φ, for EFIOR mechanism, and will be proportional to $\sin 2\varphi$, for OR mechanism. In the case of n-InAs, such experiments were performed in [15]; it has been demonstrated there that OR effect is weak and the EFIOR effect is prevailing in this material. The significance of this effect was also pinpointed in [20], when explaining the enhancement of THz emission from p-type InAs crystals.

Fig. 5 shows the dependence of the emitted THz field magnitude on the crystal doping level. It can be seen from that figure that there is a strong enhancement of the radiated field magnitude corresponding to p-type doping levels of 10^{16} to 10^{17} cm^{-3}. The strong doping level dependence of THz generation from p-InAs samples indicates that the prevailing physical mechanism of this effect is the electric-field-induced instantaneous polarization. Surface depletion

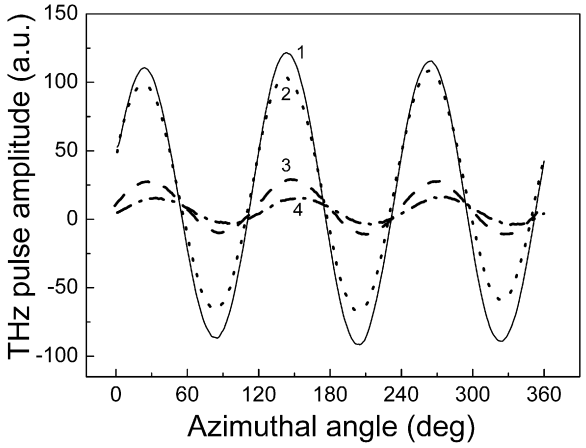

Fig. 4. The azimuthal angle dependences of the amplitude of S-polarized THz signals measured on two p-InAs (curve 1—doping level 5×10^{16} cm^{-3}, 2—2×10^{17} cm^{-3}) and two n-InAs samples (3—2×10^{16} cm^{-3}, 4—9×10^{17} cm^{-3}).

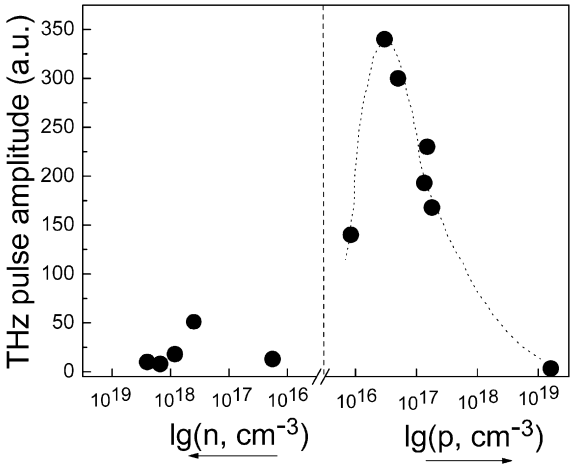

Fig. 5. Dependence of the emitted THz field magnitude on the InAs crystal doping level (dotted line is guide for eye only).

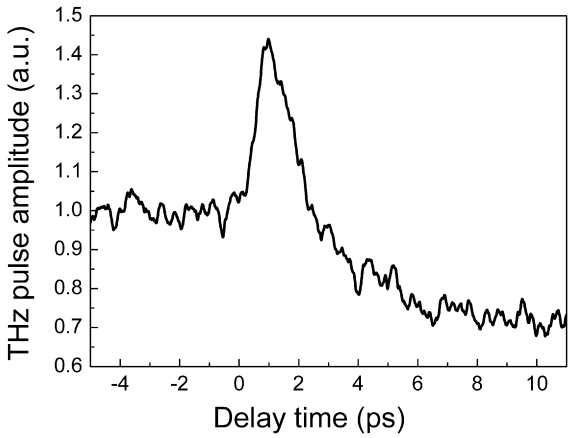

Fig. 6. *S*-polarized component of the THz signal at its maximum as a function of the time delay between the probe and pump pulses.

layer width in the samples with $p = 10^{17}$ cm^{-3} is approximately the same as the light absorption length at the laser wavelength (∼100 nm); therefore nonlinear optical interaction due to electric-field-induced optical rectification should be most efficient in this case.

A necessary condition for the EFIOR effect is a presence of a strong surface electrical field. This condition is rarely met in narrow-gap semiconductors such as InAs. On could expect the presence of such field in *p*-InAs, where the surface potential is fixed high in the conduction band and surface inversion layer is present [21], however, its origin in *n*-type crystals remained mysterious. In the following, we will show that a strong electric field that is appearing at photoexcited surfaces of InAs due to the ballistic electron movement or the photo-Dember effect can itself lead to the enhancement of the THz pulse emission via EFIOR effect. As a test of this assumption, we have investigated THz emission from InAs surface induced by two optical pulses. The laser beam was split into two parts, one of which (the probe beam) was incident on the samples surface at 45° angle and generated THz pulses monitored by the detector. The second (the pump beam) part of the laser beam was parallel to the surface normal; it was focused to a rather large spot (diameter of ∼0.5 mm) in order to avoid possible interference at the detector of THz pulses generated by both laser beams. Carrier densities of approximately 4×10^{17} cm^{-3} and 10^{18} cm^{-3} were excited by the probe and pump beams, respectively. *S*-polarized component of the THz signal at its maximum was measured as a function of the time delay between the probe and pump pulses.

Fig. 6 shows the results of the pump-and-probe experiment. THz emission increases at times close to the overlap of both optical pulses and becomes weaker when the pump pulse arrives at the sample before the probe pulse. The effect of the carriers excited by the pump pulse on THz signal generated by the probe pulse is twofold. First of all, electron ballistic movement and the charge carrier separation add to the surface electric field and lead to an increase in the generated THz signal. Secondly, when the pump pulse arrives at the surface at much earlier time moment than the probe pulse, carriers excited by the pump pulse can be already cooled-down and contribute to the relaxation of the surface electrical field and to the reduction of the THz generation. The shape of the experimental trace presented on Fig. 6 evidences the presence of both effects. The peak of THz emission at times close to the zero delay is due to the enhancement of the EFIOR contribution in the field induced by the pump pulse and the reduction of this emission at longer delays is, most probably, caused by the screening of the surface electrical field by the photoexcited carriers.

Fig. 7 presents the amplitudes of the THz signal radiated from InAs surface for different femtosecond laser quantum energies [22]. The values of the THz signal are normalized to the number of photons impinging the semiconductor at each laser wavelength. As can be seen from this figure, the dependence has a peak in the vicinity of ∼1.6 eV. This result is coincident with numerical calculations (Fig. 3). It is worthy of note that, in the range 1.6–2.2 eV of excitation quantum energies, the azimuthal angle dependent part of the THz signal decreases with the increasing quantum energy $h\nu$ even faster than the angle independent part. Most probably, free carrier enhanced nonlinear susceptibilities are affected by the intervalley scattering processes; on the other hand, these carrier scattering processes impede the establishment of the surface field as it was discussed above.

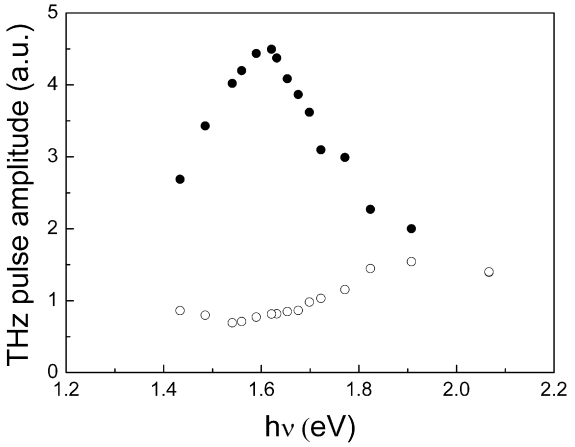

Fig. 7. THz signal radiated from InAs surface for different laser quantum energies and different azimuthal angles corresponding to minimum (open dots) and maximum (filled dots) signal amplitude.

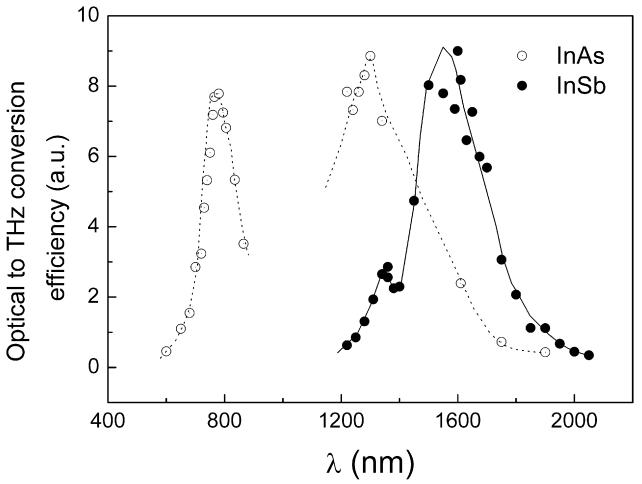

Fig. 8. Optical-to-THz power conversion efficiencies for InSb and InAs.

3.2. InSb

The question that has remained unsolved for a long time was why THz emission from InSb is much weaker than that from InAs. Indium antimonide has a narrower bandgap, a smaller effective electron mass, and higher electron mobility than InAs, therefore one would expect it to be at least as efficient THz emitter as InAs. However, THz power emitted from InSb illuminated by Ti:sapphire laser pulses ($\lambda \approx 800$ nm) surface is two orders of magnitude smaller than that emitted from InAs surface. One explanation of this contradiction could be the effect of the photoexcited electron scattering to subsidiary, high effective mass L valleys in the conduction band of InSb, where their mobility is much lower than in the main Γ valley [23]. In InAs the energy separation of Γ and L valleys is larger than in InSb [24], therefore the energy of the Ti:sapphire laser quantum is insufficient to activate the intervalley transfer processes and the electrons remain in high mobility Γ valley. We performed experiments with tunable wavelength laser system (Figs. 7 and 8) and confirmed this explanation.

For comparing different materials as prospective THz emitters, it is more convenient to plot their optical-to-THz power conversion efficiencies. Such plots for InSb and InAs are shown on Fig. 8 [22]. It can be seen from the figure that, e.g., in the practically important 1.5 μm wavelength range, InSb is a better THz emitter than InAs. Moreover, the structure of the spectra is more complex than it could be envisaged from a simple model involving the onset of the intervalley transitions. For both InSb and InAs, maxima at ∼1.3 μm additional to those explained by these transitions, were observed. If in the case of InSb this additional maximum could be explained by the intervalley transitions of the electrons excited from the light-hole valence band, then for InAs the origin of the enhanced THz emission in this spectral range is unclear and requires a further investigation.

3.3. Germanium

Sufficiently high THz emission efficiency and well-known material parameters of Ge had allowed us to approach the microscopic origin of THz emission in this material more thoroughly. The polarity of THz electrical transients was the same for n-type and p-type Ge surfaces, which suggested that the build-up of the Dember field due to the different electron and hole diffusion currents is one of the main THz generation mechanisms in this material. This field caused the restoring force and thus started oscillating motion of the charge carriers. THz spectra radiated by differently doped Ge samples shifted to the higher frequencies with increasing doping density, evidencing that this oscillation involved mainly the 'cold' plasma consisting of equilibrium electrons and holes [25].

For the measurement of the electrical transport dynamics in Ge samples on the subpicosecond time scale, the optical pump—THz probe technique was employed. Fig. 9 shows the temporal dynamics of the optically induced change in the transmittance at THz frequencies as measured by this technique [25]. Experimental traces obtained on both n- and p-type Ge samples coincide with each other within the experimental accuracy. It should be noted that the

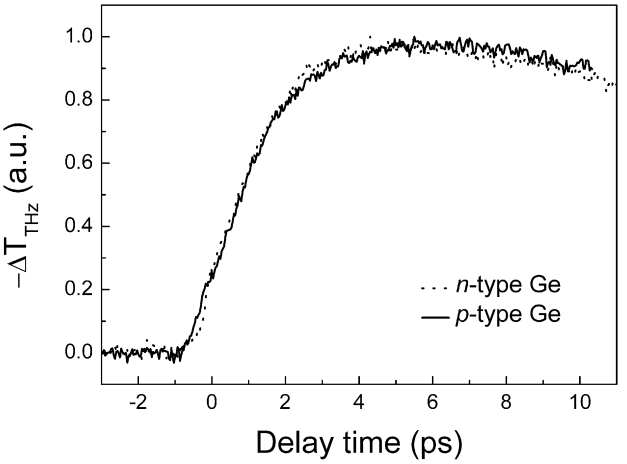

Fig. 9. The temporal dynamics of optical pump induced change in the transmittance at THz frequencies obtained on both n (dotted line) and p-type (solid line) Ge samples.

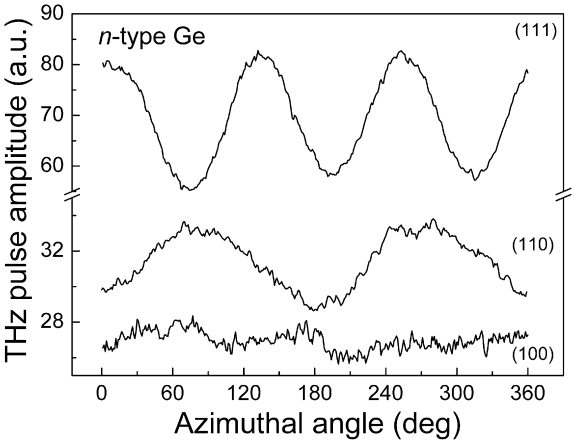

Fig. 10. The azimuthal angle dependences of THz signal amplitude measured by photoexciting three different planes of n-type Ge crystals.

rise time of the induced THz transmittance transient is unexpectedly long—several picoseconds. Similar transients when measured on such direct bandgap semiconductors as InP or GaAs usually were characterized by the rise times comparable with the temporal resolution of the experiment (∼0.5 ps). These peculiarities were explained by us [25] by a complex many-valley nature of the conduction band in Ge. Ti:sapphire laser quanta ($h\nu = 1.55$ eV) are exciting electrons high into the energy states of the central Γ minimum. From those states the electrons are first scattered to Δ-minima and, finally, to the lowest lying L-minima. Monte Carlo simulation of the transient electron mobility that was performed by taking into account these inter-valley scattering processes has led to the result closely coinciding with the experimental observations.

In [26] it has been demonstrated that the nonlinear optical processes can also contribute to the THz radiation from Ge surfaces and that this contribution can be comparable to that of the photo-Dember effect for certain experimental geometries. Fig. 10 shows the azimuthal angle dependence of THz signal amplitude measured by illuminating three different crystalline planes of n-type Ge samples. THz signal amplitude does not depend on the rotation of the crystal around the normal to its surface for (100) crystallographic plane but shows a distinct periodic dependence proportional to $\cos 3\varphi$ and $\cos 2\varphi$ for the planes (111) and (110), respectively. These observations show the presence of THz radiation caused by EFIOR effect at the laser illuminated Ge surfaces. This conclusion is further supported by the experiments performed with differently doped Ge samples. Fig. 11 presents THz signal amplitude measured as a function of the azimuthal angle on two n-type Ge and two p-type Ge crystals. In both cases, angle dependent parts of the dependences are larger for the crystals with a smaller resistivity, for which larger surface electric fields could be expected.

It is clear from the described experimental results that THz radiation from Ge surfaces excited by femtosecond laser pulses originates from two physical mechanisms: the photo-Dember effect caused by different electron and hole diffusion rates and the nonlinear optical response induced by the built-in electrical field at the crystal surface (EFIOR effect). Therefore, THz signal amplitude dependence on the azimuthal angle at, e.g., (111) plane will have the form:

$$E_{\mathrm{THz}} = E_{\mathrm{pD}} + aE_{\mathrm{s}} + bE_{\mathrm{s}}\cos(3\varphi) \quad \text{for } n\text{-type crystals and} \tag{7a}$$

$$E_{\mathrm{THz}} = E_{\mathrm{pD}} - aE_{\mathrm{s}} - bE_{\mathrm{s}}\cos(3\varphi) \quad \text{for } p\text{-type crystals} \tag{7b}$$

Here E_{pD} is the THz field amplitude due to the photo-Dember effect, E_{s} is the surface electrical field strength, a and b are constants depending on the third-order nonlinear susceptibility and other material parameters. When assuming that the surface potential is fixed at the same energy for all crystals, the average surface electrical field will be proportional to $(\rho\mu_{n,p})^{-1/2}$ (μ_n, μ_{p} are the electron and hole mobilities, ρ is the resistivity) and will have opposite sign for n-type Ge and p-type Ge. The formulae (7) can be used for determining the third-order nonlinear optical susceptibility χ_3 in germanium. We get the value of $\chi_3 \approx 10^{-8}$*CGSE*. This value is two orders of magnitude larger than previous estimations of that constant; the origin of such enhancement needs further investigation. It may

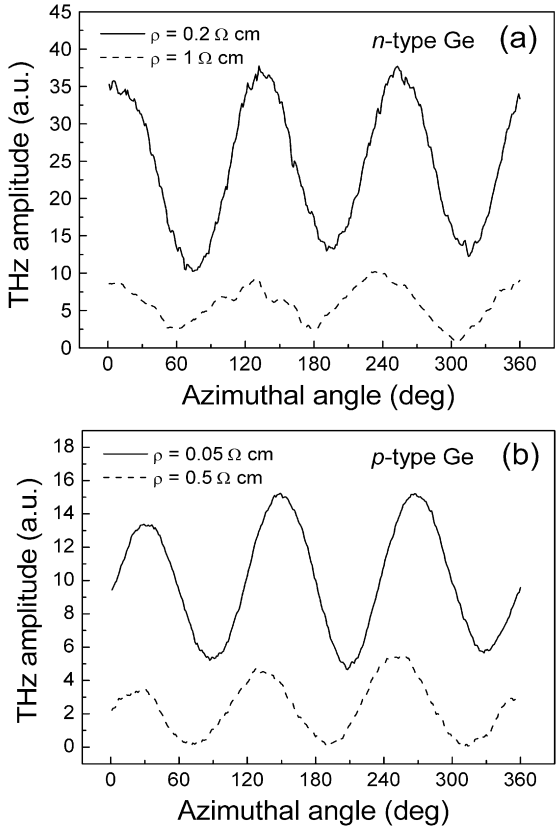

Fig. 11. THz signal amplitude measured as a function of the azimuthal angle on two n-type Ge (a) and two p-type Ge crystals (b). Curves on Fig. 11(b) are plotted on the same relative scale and displaced vertically for clarity.

be caused by the free electron contribution, which can become significantly larger than the bond electron contribution at photoexcited electron densities exceeding 10^{18} cm^{-3} [27].

3.4. Other narrow-gap semiconductors

(100) oriented $Cd_xHg_{1-x}Te$ and $In_xGa_{1-x}As$ samples excited by femtosecond Ti:sapphire laser pulses are also emitting THz radiation. No azimuthal angle dependence of the radiated signal was detected, indicating that bulk OR contribution is negligible in these cases. Terahertz fields radiated by the samples of all three investigated $Cd_xHg_{1-x}Te$ alloy compositions ($x = 0$, 0.2, and 0.3) were of the same order of magnitude and no clear dependence on x was found [28]. This experimental result was explained by the electron transitions from the spin-orbital split valence band to the conduction band.

In contrast, THz fields radiated by the $In_xGa_{1-x}As$ samples increased linearly with increasing photoelectron excess energy (Fig. 12). These results suggested the conclusion that most efficient THz emitters are semiconductors with a narrow bandgap and large intervalley separation in the conduction band.

3.5. Modified n-GaAs surface emitters

It is known that THz radiation from n-GaAs is mainly caused by the motion of photoexcited electrons and holes separated by the surface electric field [29]. This field can be enhanced by placing an additional layer of GaAs grown by molecular-beam epitaxy (MBE) at low temperature (LTG GaAs) on top of the n-doped layer. It can be expected that a thin LTG GaAs layers should ensure a firm pinning of the Fermi level in the middle of the GaAs band gap, thus increasing the emitted power of the THz radiation. Several different emitter structures were investigated [30]. The reference structure consisted of a 1.5-μm-thick Si-doped n-GaAs layer with $n = 5 \times 10^{15}$ cm^{-3} grown by MBE on

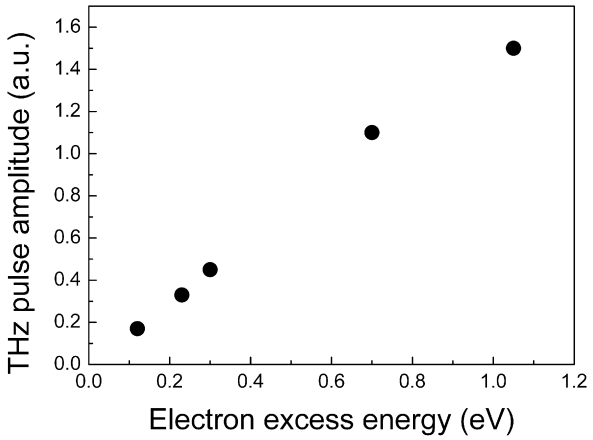

Fig. 12. THz generation from the surfaces of various compounds in InAs–GaAs system as a function of the photoexcited electron excess energy (Ti:sapphire laser).

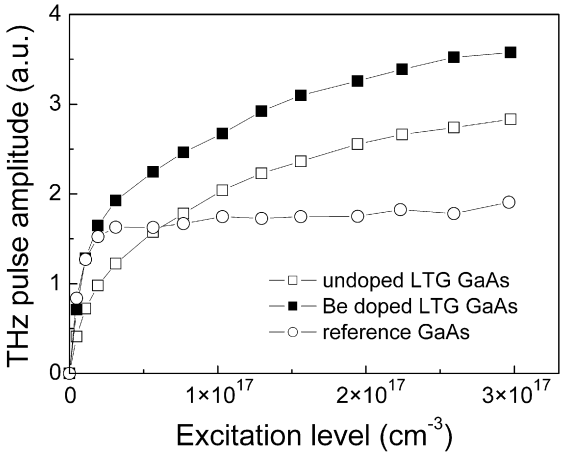

Fig. 13. Dependencies of the THz electric field magnitude (measured as the difference between the peak and valley of the experimental trace) on the optical excitation intensity.

a semi-insulating GaAs substrate. In the case of the surface-modified emitter structures, a lowering of the substrate temperature to 270 °C followed the growth of the *n*-type layer. At this temperature, LTG GaAs layers of a thickness of 60–70 nm were grown under arsenic supersaturation. In one of the wafers, the LTG GaAs layer was nominally undoped, in another this layer was doped to a nominal Be density of 5×10^{19} cm^{-3}. After growth, both wafers were split into two parts: one part was investigated as grown, another was annealed in rapid thermal annealing furnace at 600 °C for 30 s in Ar atmosphere.

In the low excitation range (photoexcited carrier density lower than 3×10^{15} cm^{-3}) the structure with an as-grown Be-doped LTG GaAs layer radiated THz transients with the greatest magnitude. The magnitude of the transients radiated by emitters with nondoped as-grown LTG GaAs and with annealed LTG GaAs was smaller than reference signal magnitude. The THz transient magnitude correlated well with the band bending in the *n*-GaAs layer. The central frequency of generated THz radiation was observed not to be dependent on the excitation power. These features of THz radiation allowed us to suggest that this radiation was due to the cold plasma oscillations from the extrinsic electrons in the *n*-doped layer. If the differences in THz transients generated by various emitter structures at low excitation levels were small and purely quantitative, at large excitation the transients started to differ also qualitatively. It can be seen from Fig. 13 that, in contrast to the reference sample whose signal saturated at relatively low excitation intensity, THz emission from the structures with a LTG GaAs layer on the top monotonously increased to the largest excitations employed. It was assumed that the observed differences for the reference sample and the sample with LTG GaAs layer were caused by different dynamics of the surface field screening by photoexcited holes [30].

4. Concluding remarks

Investigation of THz emission from semiconductor surfaces had passed its initial stage and this effect is mature for its wider application. First of all, because of its rather universal occurrence, the effect of THz radiation from femtosecond laser excited surfaces can provide unique information on such basic semiconductor properties as the electronic band structure or carrier scattering mechanisms. As a tool for material investigation, THz emission was lately used not only on semiconductors, but also for the dynamic study of ferromagnetic [31] and ferroelectric [32] materials.

Although THz pulses emitted from unbiased semiconductor surfaces are, for the time being, less powerful than the pulses generated by photoconductive antennae, there is much space for improvement by employing larger area emitters or by engineering optimized device structures from the materials with efficient THz emission. Good example of such materials could be $CuInSe_2$ and related thin-film solar cell materials, which are shown to radiate THz pulses rather efficiently [33]. Large area layers of $CuInSe_2$ can be deposited on various substrates; THz emission can be modulated and enhanced by reverse biasing the diode structures based on these materials.

References

[1] J. Shan, T.F. Heinz, in: K.T. Tsen (Ed.), Ultrafast Dynamical Processes in Semiconductors, Topics in Applied Physics, Springer-Verlag, Berlin, 2004, p. 1.
[2] X.-C. Zhang, B.B. Hu, J.T. Darrow, D.H. Auston, Appl. Phys. Lett. 56 (1990) 1011–1013.
[3] A. Krotkus, J.-L. Coutaz, Semicond. Sci. Technol. 20 (2005) S142.
[4] N. Chimot, J. Mangeney, L. Joulaud, H. Bernas, K. Blary, J.F. Lampin, Appl. Phys. Lett. 87 (2005) 193510.
[5] K.G. Wilcox, F. Rutz, R. Wilk, H.D. Foreman, J.S. Roberts, J. Sigmund, H.L. Hartnagel, M. Koch, A.C. Tropper, Electron. Lett. 42 (2006) 1159.
[6] K. Bertulis, A. Krotkus, G. Aleksejenko, V. Pačebutas, R. Adomavičius, G. Molis, S. Marcinkevičius, Appl. Phys. Lett. 88 (2006) 201112.
[7] T. Dekorsy, T. Pfeifer, W. Kutt, H. Kurz, Phys. Rev. B 47 (1993) 3842.
[8] R.W. Hockney, J.W. Eastwood, Computer Simulation Using Particles, McGraw–Hill, New York, 1981.
[9] V.L. Malevich, Semicond. Sci. Technol. 17 (2002) 551.
[10] R. Kersting, K. Unterrainer, G. Strasser, H.F. Kaufmann, E. Gornik, Phys. Rev. Lett. 79 (1997) 3038.
[11] V.L. Malevich, Semiconductors 40 (2006) 155.
[12] V.I. Zemskii, B.P. Zakharchenia, D.N. Mirlin, JETP Pisma 24 (1976) 96.
[13] V.L. Alperovich, V.I. Belinicher, V.N. Novikov, A.S. Terekhov, JETP Pisma 31 (1980) 581.
[14] V.L. Alperovich, V.I. Belinicher, V.N. Novikov, A.S. Terekhov, JETP 80 (1981) 2298.
[15] M. Reid, I.V. Gravetchi, R. Fedosejevs, Phys. Rev. B 72 (2005) 035201.
[16] J.J. Wynne, N. Bloembergen, Phys. Rev. 188 (1969) 1211.
[17] J.J. Wynne, Phys. Rev. 188 (1969) 1295.
[18] J.B. Khurgin, J. Opt. Soc. Am. B 11 (1994) 2492.
[19] J.E. Sipe, A.I. Shkrebtii, Phys. Rev. B 61 (2000) 5337.
[20] R. Adomavičius, A. Urbanowicz, G. Molis, A. Krotkus, E. Šatkovskis, Appl. Phys. Lett. 85 (2004) 2463.
[21] C. Affentaugscheggl, H.H. Wieder, Semicond. Sci. Technol. 16 (2001) 708.
[22] R. Adomavičius, G. Molis, A. Krotkus, V. Sirutkaitis, Appl. Phys. Lett. 87 (2005) 261101.
[23] S.C. Howells, S.D. Herrera, L.A. Schlie, Appl. Phys. Lett. 65 (1994) 2946.
[24] A. Krotkus, Z. Dobrovolskis, Electrical Conductivity of Narrow-Gap Semiconductors, Mintis, Vilnius, 1988.
[25] A. Urbanowicz, R. Adomavičius, A. Krotkus, V.L. Malevich, Semicond. Sci. Technol. 20 (2005) 1010.
[26] A. Urbanowicz, A. Krotkus, R. Adomavičius, V.L. Malevich, Physica B: Condens. Matter 398 (2007) 98–101.
[27] C.C. Wang, N.W. Ressler, Phys. Rev. 188 (1969) 1291–1293.
[28] A. Krotkus, R. Adomavičius, G. Molis, A. Urbanowicz, H. Eusebe, J. Appl. Phys. 96 (2004) 4006–4008.
[29] M.B. Johnston, D.M. Whittaker, A. Corchia, A.G. Davies, E.H. Linfield, Phys. Rev. B 65 (2002) 165301.
[30] K. Liu, A. Krotkus, K. Bertulis, J. Xu, X.-C. Zhang, J. Appl. Phys. 94 (2003) 3651–3653.
[31] N. Kida, M. Tonouchi, Appl. Phys. Lett. 78 (2001) 4115–4117.
[32] K. Takahashi, M. Tonouchi, Appl. Phys. Lett. 90 (2007) 052908.
[33] R. Adomavičius, A. Krotkus, J. Kois, S. Bereznev, E. Mellikov, Appl. Phys. Lett. 87 (2005) 191104.